

Synthetic and field-based electrical imaging of a zerovalent iron barrier: Implications for monitoring long-term barrier performance

Lee Slater¹ and Andrew Binley²

ABSTRACT

We performed a study of electrical imaging sensitivity to geochemical alteration of a zerovalent iron permeable reactive barrier (PRB) over time. Complex-resistivity measurements of laboratory cores from an operational PRB defined the electrical properties of both unreacted and geochemically altered (reacted) iron, as well as the growth rate of the reacted front on the up gradient edge of the barrier. Laboratory results were used to generate models of the electrical structure of the PRB at 0, 15, and 30 years of operation. Synthetic cross-borehole resistivity and induced-polarization data were generated and perturbed with errors representative of noise at the site. To generate reliable images of the engineered structure, a complex-resistivity inversion was employed with a disconnect in the regularization between the part of the finite-element mesh (FEM) representing the internal structure of the barrier and the remainder of the FEM mesh.

Synthetic results show that although the internal structure of inverted images at 15 and 30 years does not accurately reflect the width of the reacted front, modeled along the up-gradient edge of the barrier, perturbations to the internal structure of the imaged PRB are diagnostic of the growth of the reacted front. Cross-borehole electrical data, obtained at the field site during a 15-month period, demonstrate that the complex-resistivity algorithm can resolve reliably the PRB target using the engineering design specifications to define the correct shape of the regularization disconnect. Both resistivity and induced-polarization reciprocal errors are low, and the induced-polarization data are highly repeatable over this period. Changes in the electrical properties of the PRB over time were small but consistent with growth of a reacted front, based on the synthetic study. Significantly, resistivity imaging alone may be sufficient for long-term monitoring of precipitation, leading to reduced PRB performance.

INTRODUCTION

The permeable reactive barrier (PRB) is an innovative in-situ technology for the remediation of chlorinated hydrocarbon, heavy metal, or radionuclide contaminated groundwater (Gilham and O'Hannesin, 1994; Gu et al., 1998; Vogan et al., 1999). The reactive material of the barrier participates in a redox reaction with the contaminant, resulting in the conversion of the contaminant into inorganic, nontoxic compounds. The reactive zerovalent iron (Fe⁰) barrier is the most established PRB technology for the in situ remediation of chlorinated solvents as well as heavy metals. For example, degradation of trichloroethylene (TCE) by Fe⁰ is assumed generally to result in ethene and chloride as the primary end products (Gavaskar et al., 1998).

As of 2002, 80 Fe⁰ barriers were identified operating worldwide (Carey et al., 2002). Although many of these barriers currently meet design specifications, concern exists regarding long-term (decade-scale) performance reduction as a result of oxidation and precipitation at the zerovalent iron (Fe⁰) surface (Liang et al., 2000; Phillips et al., 2000; Furukawa et al., 2002; Kohn et al., 2005), as well as clogging of the pore space (Mackenzie et al., 1999). Laboratory and field experiments have investigated the nature and rates of corrosion and precipitation and/or clogging in Fe⁰ barriers (Gu et al., 1999; Liang et al., 2000; Phillips et al., 2000; Furukawa et al., 2002; Klausen et al., 2003; Liang et al., 2003; Kohn et al., 2005). It is well recognized that field-scale technologies are required to monitor and provide warning of performance reduction, permitting remedial measures to

Manuscript received by the Editor August 18, 2005; revised manuscript received January 22, 2006; published online August 28, 2006.

¹Rutgers University, Department of Earth and Environmental Sciences, 195 University Avenue, Newark, New Jersey 07102. E-mail: lslater@andromeda.rutgers.edu.

²Lancaster University, Department of Environmental Science, Lancaster, LA1 4YQ, United Kingdom. E-mail: a.binley@lancaster.ac.uk.

© 2006 Society of Exploration Geophysicists. All rights reserved.

reduce contaminant concentrations at locations down gradient from the barrier site.

Previous workers have recognized the potential of geophysical tools to help investigate PRBs installed at contaminated sites. Geophysical imaging methods can potentially provide in-situ information on the internal properties of the barrier without compromising the integrity of the engineered structure. Joesten et al. (2001) conducted crosshole radar imaging of pilot-scale testing of a hydraulic fracture method of PRB installation in unconsolidated sediments at depth. Crosshole radar amplitude measurements between 14 boreholes were combined to define variability in cross-sectional amplitude attenuation along the length of the two walls. Small-scale structures were interpreted tentatively as stringers of iron possibly attributable to iron particles moving into higher-permeability formations. More recently, Slater and Binley (2003) describe an application of electrical imaging at a Fe^0 PRB installation in Kansas City, Missouri. They showed that electrical imaging could visualize the structure of this PRB after installation. Variations in electrical images along the length of the barrier were interpreted as evidence for flaws originating during the construction and emplacement of the barrier.

The focus of this paper is to expand upon a concept noted by Slater and Binley (2003): Electrical imaging might be used to monitor the long-term health of a permeable reactive barrier. The basis of this argument is that corrosion/precipitation and/or clogging will alter the electrical properties of the PRB. Slater et al. (2005) reported laboratory experiments on Fe^0 columns to support this concept: The complex conductivity of Fe^0 columns showed a significant increase in both real and imaginary parts of the complex conductivity following precipitation of iron hydroxides and iron carbonates (see Figure 7 of Slater et al., 2005).

In this paper, we utilize the results of laboratory geochemical and geophysical measurements on cores obtained from the Kansas City PRB. We determine the likely changes in the electrical properties of this barrier associated with alteration of the iron surface over time. This information is used to generate synthetic realizations of the modified PRB structure upon installation and at 15 and 30 years after completion. These data sets are inverted using a regularization constraint that satisfies the structure of the PRB (in our case, from design specifications that must accurately represent the in-situ geometry of the PRB) and results in plausible geophysical images of the electrical changes inside the PRB with time. The synthetic runs are compared with the results of 15 months of monitoring at the Kansas City site.

ELECTRICAL IMAGING

Tomographic electrical imaging is an established technology for visualizing the geoelectrical structure of the subsurface (Daily and Owen, 1991; Park and Van, 1991; Shima, 1992; Oldenburg and Li, 1994; LaBrecque et al., 1996). Numerous environmental applications of the technology are reported, including monitoring of leaks from underground storage tanks (Ramirez et al., 1996), detection of unexploded ordnance (Daily et al., 2000), and imaging hydraulic barriers (Daily and Ramirez, 2000). Apparent conductivity and IP measurements are made for many sets of four electrodes placed in boreholes or at the surface. Given these measurements, it is possible to solve numerically for conductivity and IP distributions that result in a set of calculated measurements best fitting with the measured response. The numerical calculations involve 2D or 3D forward mod-

eling [in this work using the finite-element (FE) method]. In the case of a 2D model, it is implicitly assumed that the electrical structure in the third dimension is constant. A 2D model was used in this study because the barrier is a 2D target at the image planes shown in Figure 1 (i.e., the cross-sectional PRB structure is continuous along the length of the barrier). Although some heterogeneity within the barrier undoubtedly exists (as evidenced by small sand inclusions observed in one core from the barrier described below), we assume that the 2D assumption holds well at the scale of the image resolution.

The inversion algorithm utilized here is based on an Occam's-type procedure (de Groot Hedlin and Constable, 1990) with one significant modification noted below. To perform the IP inversion, we utilize a complex-conductivity algorithm first outlined by Kemna and Binley (1996) and described in detail by Kemna (2000). Kemna et al. (2004) provide further details of the modeling approach and give examples to illustrate how the approach can be used for cross-borehole IP investigations. The algorithm requires measurements of the magnitude ($|\sigma|$) and ϕ of the conductivity as input data. However, because of the equivalence between field and normalized IP parameters, we can substitute field measures of M for ϕ , obtaining images of ϕ and imaginary conductivity scaled by a constant (for full details, see Slater and Binley, 2003). Inversion of the ratio of two electrical data sets scaled by a numerical forward solution based on a homogeneous model is a technique for imaging changes over time that avoids the large propagation of error resulting when inverted data sets from two times are subtracted directly (e.g., Slater et al.,

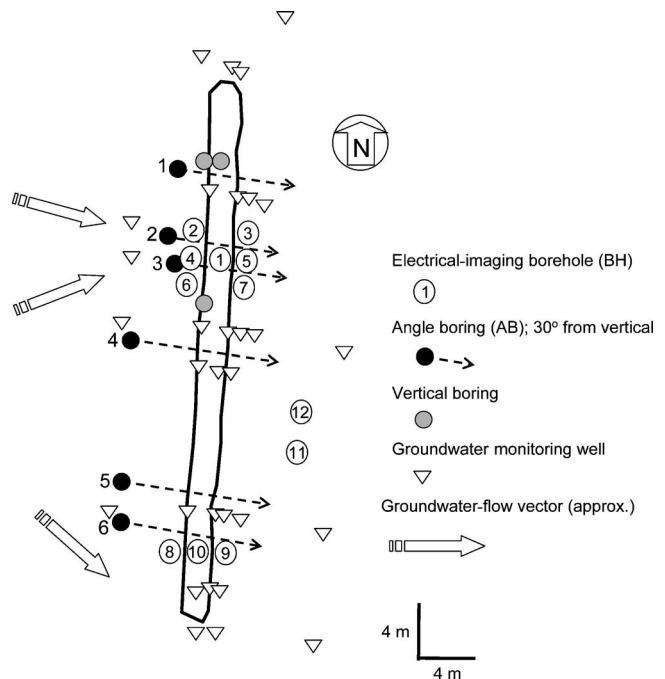


Figure 1. Plan view of Kansas City PRB site, showing the outline of the PRB, location of electrical imaging boreholes (BH), 30° from vertical angle borings (with direction), vertical borings, groundwater monitoring wells, and the approximate groundwater-flow vector. BH11 and BH12 are located off the barrier and form a control image panel. Note that the electrical-imaging boreholes used in our previous work conducted during 2001–2002 and reported in Slater and Binley (2003) were back-filled per site regulations in 2002. These new boreholes do not relate in any way to those referenced in Slater and Binley (2003).

2000). We applied this ratio approach in addition to the direct inversion of complex-conductivity terms.

As in most conventional inversions with smoothness regularization, the objective function, which is minimized, combines the data misfit (the error between observed data and modeled response for a given electrical structure) and the model roughness. The model roughness acts as a penalty function to ensure that the data are not fit at the expense of producing an unrealistically rough structure within the image while enhancing the stability of the inversion. This form of regularization may be argued on the grounds that electrical properties of the subsurface often are expected to vary spatially in a smooth fashion. However, for the case of engineered structures such as PRBs, we expect relatively sharp contrasts in electrical properties at the boundaries of the structure and the host geology.

To address this, we incorporate a regularization constraint to satisfy the structure of the PRB (from design specifications) and help the inversion to find plausible geophysical images of the internal structure of the PRB at different times. The outline of the barrier (Figure 2) is used to define a disconnect in the regularization (spatial smoothing) between the part of the FE mesh (FEM) representing the internal structure of the barrier and the remainder of the FEM. The off-diagonal elements of the roughness matrix (Binley and Kemna, 2005), which control the smoothing of the image, are removed for parameters in the image that are located along the barrier boundary. This means that the regularization (essential for stability of the inversion) does not introduce any smoothing across the boundary of the barrier. Therefore, the values of the inversion parameters, representing the internal structure of the barrier, cannot be influenced through the regularization by the values of the inversion parameters comprising the remainder of the image. We note that the effectiveness of this approach relies on accurate ground-truth information on the shape of the barrier, i.e., in our case, that the design specifications for the shape of the barrier were achieved during installation. This is

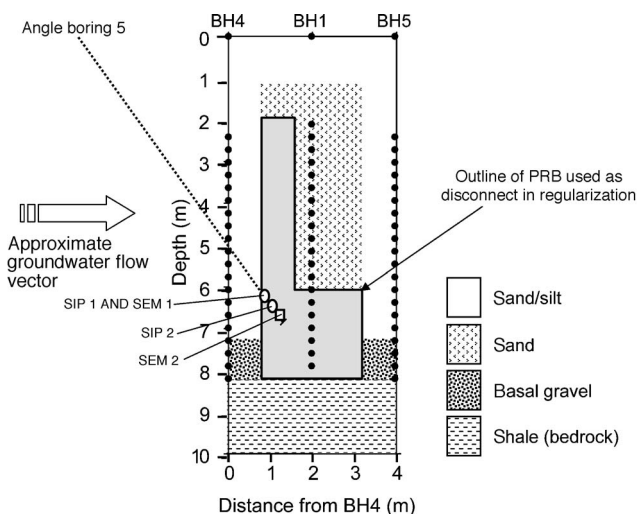


Figure 2. Cross section of image plane BH4, BH1, and BH5 showing the outline of the iron barrier per design specifications, basic geology, and position of electrodes (solid circles) used for electrical imaging. Each borehole (BH) contains 21 electrodes, including the electrode placed at the ground surface. The size of the FEM used to model the electrical data within the region bound by the borehole electrodes is 0.2 m in the horizontal and 0.076 m in the vertical. Location of angle boring BH5 in cross section is also shown (note that angle boring 5 is offset 17 m south of this image plane).

justified because we are concerned with imaging changes in the internal properties of an established structure over time.

STUDY SITE

The PRB under study was installed in April 1998 at the U. S. Department of Energy's Kansas City Plant in Kansas City, Missouri (U. S. Department of Energy, 2003). It was designed to remediate 1,2-dichloroethylene (1,2-DCE) and vinyl chloride (VC) in contaminated groundwater migrating from the facility. Figure 1 is a plan view of the site, showing the outline of the PRB, location of electrical imaging boreholes (BH) used for long-term monitoring, vertical and angle coring locations, and groundwater monitoring wells. The PRB was constructed as a continuous 40-m (130-ft) long, 1.8-m (6-ft) wide trench. Figure 2 shows a cross-sectional view of the barrier geometry, site geology, and the location of electrodes in the plane BH4-BH1-BH5. Alluvial sediments underlie the site — primarily silty clay overlying basal gravel. These alluvial sediments are underlain by bedrock shale. The PRB was constructed by filling the first 1.8 m (6 ft) of the trench with 100% zerovalent granular iron so that the base of this section was in contact with bedrock. The remainder of the trench was then filled with 0.6 m (2 ft) of zerovalent iron and 1.2 m (4 ft) of sand (Figure 2). The thicker, lower unit was designed to compensate for the higher flow-through velocities associated with hydraulically conductive basal gravel that rests on bedrock (Figure 2).

The performance of the Kansas City PRB has been affected adversely by alteration to groundwater flow near the PRB, resulting from the installation of the PRB structure itself (DOE, 2003). Hydraulic head measured at the network of 27 monitoring wells at the site (Figure 1) shows that part of the plume is bypassing the barrier by flowing around its southern edge (Figure 1). This seems to reflect reduced hydraulic conductivity of the barrier associated with a clay smear zone that was attached to the barrier's up-gradient edge during installation. Geochemical measurements show incomplete removal of organic compounds in the monitoring wells down gradient of the barrier near its southern end, presumably reflecting this plume movement around the southern edge of the barrier (U. S. Department of Energy, 2003).

These issues influenced the design of the electrical imaging experiments conducted at the site. Twelve electrode arrays were installed at the site during January 2003. Note that the electrical-imaging boreholes used in our previous work conducted during 2001–2002 and reported in Slater and Binley (2003) were backfilled according to site regulations in 2002 (i.e., these new wells do not relate to those referenced in Slater and Binley, 2003). Boreholes 1–7 were installed at the location where groundwater flow through the barrier is concentrated and the greatest changes in electrical properties should be expected. BH4-BH1-BH5 defines the primary 2D image plane for monitoring. The additional boreholes were installed at this site to test imaging of the barrier structure in three dimensions. A second 2D image plane (BH8-BH10-BH9) was established for comparative purposes toward the southern end of the barrier where groundwater flow through the PRB is reduced. Image plane BH11-BH12 was established as a control off the barrier.

Each borehole consisted of 20 electrodes spanning the height of the barrier, plus one electrode placed at the ground surface. Boreholes 1 and 10 were drilled at the center of image planes BH4-BH1-BH5 and BH8-BH10-BH9, therefore penetrating the lower segment of the PRB (Figure 2). Lead electrodes were used in this study. Ideal-

ly, we would have used a nonpolarizing electrode such as a Pb-PbCl junction, but excessive costs and awkward implementation in boreholes negated this approach. Regular metal electrodes can give IP measurements of similar quality to those obtained with metal-electrolyte junction electrodes when the instrumentation such as used here incorporates data processing to remove electrode polarization at the potential electrodes (Dahlin et al., 2002). Reciprocity checks reported later testify to high-quality data achieved with these electrodes. Electrical measurements were made on image planes BH4-BH1-BH5 and BH8-BH10-BH9 on seven occasions over a 29-month period (January 2003, July 2003, November 2003, March 2004, July 2004, January 2005, and May 2005). Measurements utilizing additional electrode pairs were made less frequently; measurements on control panel BH11-BH12 were obtained on three occasions: July 2003, November 2003, and May 2005.

SUPPORT DATA

Immediately following completion of the May 2005 data set, vertical and angle borings were conducted at the site in an effort to retrieve samples of zerovalent iron for geochemical and geophysical laboratory analyses. The primary objective was to determine the width of the reacted zone on the up-gradient edge of the barrier and its electrical signature relative to unreacted zerovalent iron. Three vertical borings were conducted at the up-gradient edge of the barrier at the locations shown in Figure 1. Six angle borings (the angle of the drill bit was 30° from vertical) were also conducted, and the locations in the plan again are shown in Figure 1. The angle borings provided a sequence of core through the up-gradient interface of the barrier and into its center.

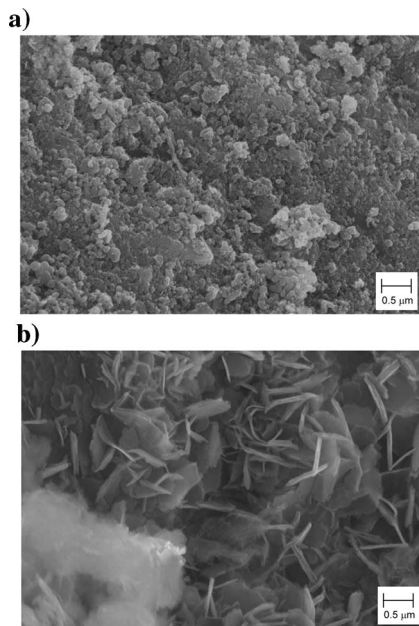


Figure 3. Scanning electron microscopy (SEM) images from samples of angle-boring 5 (a) SEM2 showing unreacted zerovalent iron sampled at 50 cm from the up-gradient interface; (b) SEM1 showing core material from the reacted zone sampled 7.5 cm from the up-gradient interface showing heavy precipitates formed on the zerovalent iron surface (sample location coincident with core measurement location SIP1 in Figure 4). Sample locations shown in cross section in Figure 2.

Laboratory analyses were conducted on angle borings (AB) 1, 5, and 6 because the cores retrieved from AB 2–4 were cut close to the up-gradient interface, preventing accurate laboratory electrical measurements on this critical core section. The laboratory measurements along the core included (1) complex conductivity measurements from 0.1–1000 Hz of 3-cm sections, (2) scanning electron microscopy (SEM) imaging of samples, (3) X-ray diffraction measurements, and (4) sulfur and carbonate analysis.

We report three important findings required to conduct our synthetic modeling. Ideally, we would illustrate results for AB 1 because it is the closest of the three cores analyzed to our primary image plane. However, we show results obtained for AB 5 because AB 1 contained an anomalous zone of sand approximately 20 cm into the core (results obtained for AB 6 are consistent with AB 5).

First, SEM images confirm the presence of a reacted zone developing from the up-gradient edge of the Kansas City PRB. Figure 3a shows an SEM image for a sample extracted 50 cm toward the end along AB 5 (Figure 2). The image is consistent with unreacted zerovalent iron within the barrier and away from the up-gradient edge. Figure 3b shows the SEM image for the sample extracted at 7.5 cm along PRB 5. Here the SEM image reveals heavy precipitates formed on the iron surface. The results of X-ray diffractometry, as well as the hexagonal platelet structure observed with SEM, suggest that these precipitates are a mixture of green rusts (a mineral phase of mixed Fe²⁺/Fe³⁺ oxy (hydroxide) layers with anions (i.e., Cl⁻, CO₃²⁻, and SO₄²⁻) incorporated into inner-layer spaces) and iron oxyhydroxides. Such minerals have been identified as precipitates in other zerovalent iron barriers (Legrand et al., 2001; Su and Puls, 2004).

Second, complex-conductivity data illustrate the magnitude of change in electrical measurements, expected as a result of the mineralogical alteration identified in Figure 3. Figure 4 shows the complex-conductivity response from 0.1–1000 Hz at two locations along AB 5: (a) SIP1 is within the reacted zone, 7.5 cm from the up-gradient interface and coincident with the location of SEM1; (b) SIP2 is from deeper within the barrier — 50 cm from the up-gradient interface — coincident with SEM2 and representing unreacted zerovalent iron. Both samples were fully resaturated with site groundwater ($\sigma_w = 0.81$ mS/cm): In each case the sample length is 3 cm, and the sample diameter is 2.14 cm. These measurements show that the mineralogical alteration in the reacted zone increases the real and imaginary parts of the complex conductivity. Results from AB 6 confirm this finding; furthermore, we have observed similar changes in laboratory cores treated with synthetic groundwater to induce accelerated aging (Wu et al., 2005).

In all cases, the changes in the electrical properties attributed to the corrosion-precipitation process are orders of magnitude larger than changes in the electrical properties observed resulting from differences in packing of granular Fe⁰ (Wu et al., 2005). Modeling of these complex conductivity data sets obtained on these cores and detailed discussion of the electrochemical mechanisms causing the increase in complex conductivity are subjects of a separate paper.

For our current work, we are most interested in defining the likely change in the measured real and imaginary conductivity at low frequencies representative of single-frequency, field-scale induced-polarization measurements as a result of the mineralogical alteration associated with aging. Arbitrarily assigning a 1-Hz measurement frequency, Figure 4 shows that the real conductivity increases by approximately one order of magnitude from 0.1 S/m to 1.0 S/m and the imaginary conductivity increases from approximately 0.04 S/m to about 0.1 S/m within the reacted zone. Finally, the angle borings

were used to assess the width of the reacted zone at the Kansas City barrier. From SEM analyses and visual inspection of the bores, the average horizontal width of the reacted zone during sampling in May 2005 was found to be approximately 10 cm.

SYNTHETIC STUDIES

Figure 5 shows three synthetic models and corresponding inversion results designed to test our concept of long-term monitoring of PRBs for signs of reduced barrier performance based on the Kansas City PRB. The structure (outline) of the barrier is based on the PRB design specifications given in Figure 2. Representative values for σ' and σ'' within the barrier are derived from the laboratory measurements on the angle borings.

Using Figure 4, we assigned $\sigma' = 0.1$ S/m and $\sigma'' = 0.05$ S/m for unreacted Fe⁰ saturated with in-situ groundwater. We assigned the respective values for the reacted front at the up-gradient edge of the barrier as $\sigma' = 1.0$ S/m and $\sigma'' = 0.1$ S/m (again from Figure 4). The width of the reacted front forming on the barrier's up-gradient edge was calculated based on our laboratory observation that the reacted front at the KC PRB is approximately 10 cm wide after 8 years of operation. We assumed a constant propagation rate of this reacted front to model the barrier at time (t) = 0 years (Figure 5a), $t = 15$ years (Figure 5b), and $t = 30$ years (Figure 5c) after inception. These times were selected to represent the long-term decadal scale of anticipated PRB operation (Gavaskar et al., 1998).

All inversions were performed on synthetic data based on the measurement scheme that was applied in the field monitoring at the Kansas City site. The complete data set consisted of 3744 measurements in which current and voltage dipoles were split between BH4,

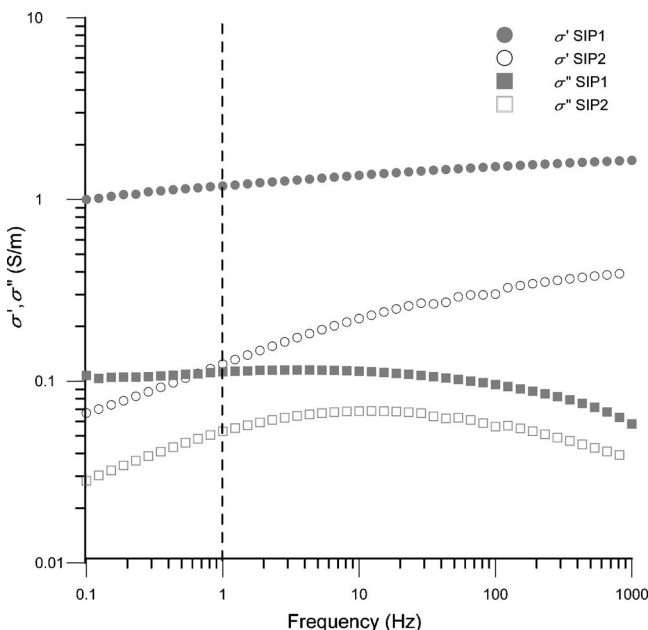


Figure 4. Comparison of electrical measurements on angle boring 5 (a) within the reacted zone 7.5 cm from the up-gradient interface (SIP1) and (b) unreacted Fe⁰ (SIP2) from deeper within the barrier (50 cm from the up-gradient interface). Both cores were fully resaturated with site groundwater ($\sigma_w = 0.81$ mS/cm) prior to electrical measurements. The dashed line denotes the measurement frequency (1 Hz) used in the synthetic and field studies. The location of the measurements on angle boring 5 is shown in Figure 2.

BH1, and BH5 (1248 measurements using BH4-BH1, 1248 measurements using BH1-BH5, and 1248 measurements using BH4-BH5). This configuration only uses measurements in which electrodes are split between two boreholes, each containing a current electrode and a potential electrode. The advantage of using such a configuration is that recorded voltages are typically higher — improving the S/N ratio of field data — than those recorded when both potential and/or both current electrodes are in the same hole. The measurements were ordered so that at no time was a voltage measured using an electrode that was previously used in the sequence to inject electrical current.

To make the synthetic tests as consistent with the field data as possible, we used only the measurements that were retained in the field data set after removing outliers based on strict reciprocity criteria, defined in the following section. The data set was filtered further to remove any measurement configurations with numerical model errors greater than 2%. This was achieved by performing a forward calculation of theoretical apparent resistivities for a homogeneous medium (the difference between the calculated apparent resistivity and the homogeneous medium resistivity is the numerical model error). The data processing resulted in the loss of approximately 15% of the measurements made between BH4-BH5 — 21% of those made between BH1-BH5 and 50% of those made between BH1-BH4. The greater rejection of data points obtained between BH1-BH4 results from the significantly lower voltages (hence lower S/R ratio) recorded on this panel as a result of the relatively greater area of conductive Fe⁰ filling this image plane. The final data set consisted of 2223 measurements that were contaminated with random noise representative of error levels in the retained field data, a standard deviation of 0.05 (fractional error) in the resistance, and a standard deviation of 1 mV/V (absolute error) in the chargeability.

Figure 5a illustrates that the unreacted, homogeneous Kansas City PRB at the time of installation is well resolved by the inversion. The real and imaginary conductivity images both accurately reproduce the model structure, and the inverted images are devoid of significant artifacts. However, the inversion is unable to resolve accurately the more challenging target of a heterogeneous PRB as modeled at $t = 15$ years.

Instead, the inversion provides an alternative model that still satisfies the data misfit and model misfit constraints. Artifacts therefore appear in the inverted image (Figure 5b). Considering first the σ' image, the 20-cm wide strip ($\sigma' = 1.0$ S/m) representing the reacted zone on the up-gradient edge of the barrier is smoothed and imaged as an approximately 80-cm wide strip of variable σ' , approximately 0.2–0.4 S/m. In comparison, we are unable to resolve evidence for the reacted zone $\sigma'' = 0.1$ S/m in the σ'' image. This is somewhat disappointing because several synthetic measurements exhibit significant phase changes as a result of the modeled reaction front. However, whereas the σ' contrast between the reacted and unreacted zones is 10:1, the σ'' contrast between the reacted and unreacted zones is only 2:1.

Instead, the alternative model produced by the inversion maps artifacts both within and outside of the PRB structure. Artifacts (lower σ'') are pronounced along the up-gradient edge of the PRB where the thin layer exists. The results at $t = 30$ years are similar to those at $t = 15$ years, except that the wider 40-cm strip representing the reacted front in the model results in higher σ' (approximately 0.2–0.6 S/m) in the approximately 80-cm wide strip reconstructed by the inversion (Figure 5c). Both the σ' and σ'' images, at $t = 15$ years and $t = 30$ years, contain some artifacts whereby high

values representative of the PRB are reconstructed immediately outside of the PRB structure.

FIELD STUDIES

The measurement scheme in the field monitoring was described in the previous section. Field data were collected with a Syscal Pro 10-channel time-domain resistivity/induced-polarization instrument manufactured by Iris Instruments of France. The current waveform consisted of a 1-s injection/1-s off cycle, and the chargeability was calculated from the integral of the decay curve between 0.02 s and 0.83 s during the off cycle.

We limit our presentation of the results from image plane BH4-BH1-BH5 because changes during the monitoring period were very small but most pronounced on this image plane where flow through the barrier was focused (Figure 1).

Figure 6a, b, d, and e shows histograms of the resistance and chargeability reciprocal errors after removal of outliers in the data in the March 2004 and May 2005 data sets for image plane BH4-BH1-BH5, respectively. Outliers were defined based on the following criteria: (1) measurements that exceed a 0.05 fractional resistance error; (2) chargeability less than 10 mV/V measurements that exceed an absolute error of 1 mV/V (3) chargeability greater than 10 mV/V measurements exceeding a fractional error of 0.1. The resistance errors in Figure 6 are plotted as a fractional error whereas the IP errors are plotted as absolute values of chargeability. The mean μ and standard deviation σ_d of the data sets — calculated assuming a normal distribution (superimposed on the data in Figure 6) — are shown as annotations on the histograms plotted in Figure 6. These plots indicate that 95% of the measurements in the March 2004 and May 2005 data sets have a fractional resistance error ≤ 0.016 and an absolute chargeability error ≤ 0.98 mV/V. Figure 6 also shows the differences in the resistance (Figure 6c) and chargeability (Figure 6f) measurements between the March 2004 and May 2005 data sets for all common measurements. The scale of Figure 6c differs from Figure 6a and b because the difference between the data sets is significantly greater than the reciprocal errors within the individual data sets. Approximating the normal distribution, 60% of the fractional differences between the resistance data sets exceed 0.016. However, unlike the case of the synthetic studies, the differences in the chargeability measurements between the two data sets are not significantly greater than the reciprocal errors within each data set (compare histogram and normal distribution statistics for Figure 6f with those of Figure 6d and e).

Noise parameters in the inversion again were specified as a standard deviation of 0.05 (fractional error) in the resistance and a standard deviation of 1 mV/V (absolute error) in the chargeability. Inverted electrical images for the field data are shown in Figure 7. The complex conductivity inversion for the March 2004 data set is shown as phase angle in Figure 7a, and real and imaginary parts of the complex conductivity in Figure 7b. As explained above, there is a linear scaling applied to σ' and ϕ images here because of the use of chargeability in the complex inversion. The PRB structure is generally well resolved by the inversion, although an artifact exists outside of the barrier between 3 and 6 m deep toward the center of the image plane. All three electrical parameters reveal a generally uniform PRB structure, although there is greater variation in the σ' than σ'' inside the barrier.

Figure 7c shows a ratio image in terms of a percentage change in real conductivity between the

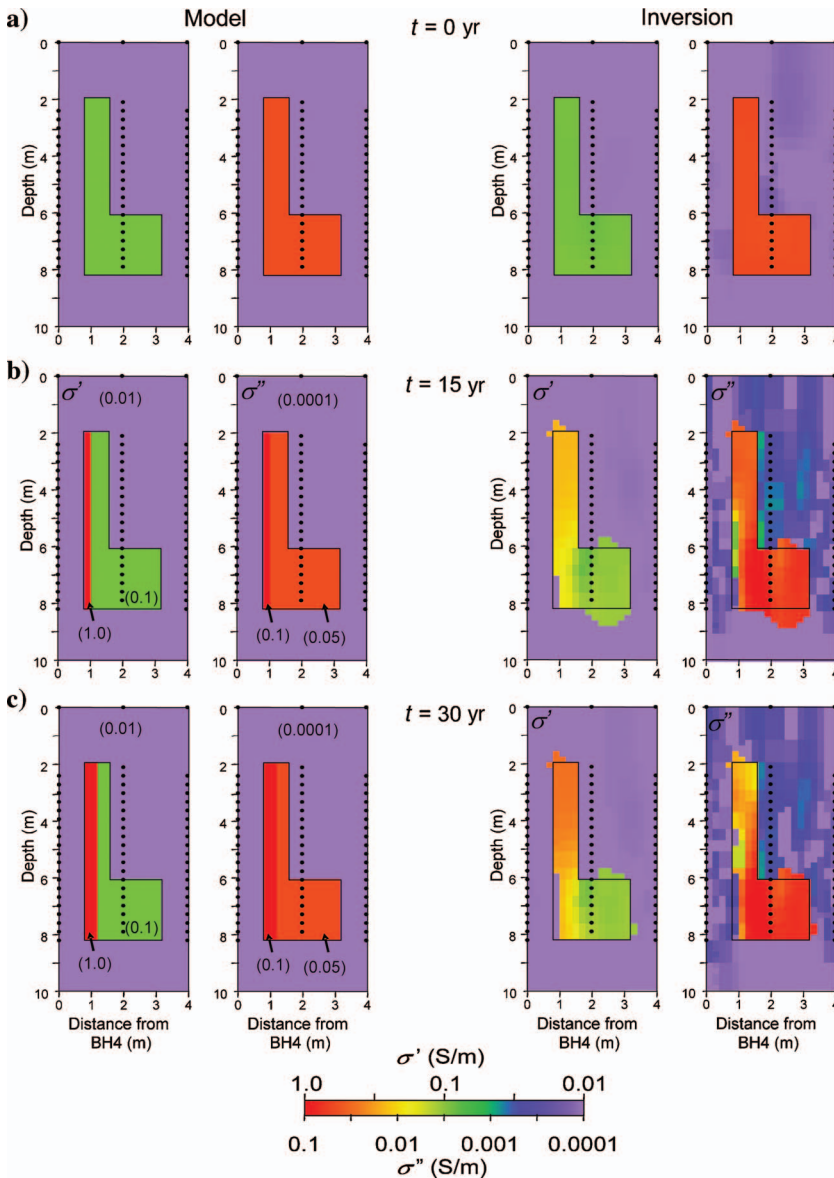


Figure 5. Synthetic models and inversion results for the Kansas City PRB at (a) $t = 0$ years, (b) $t = 15$ years, and (c) $t = 30$ years for image plane BH4, BH1, and BH5. The reacted zone is modeled as a thin strip forming on the up-gradient edge of the barrier (Figure 2). The width of the strip at $t = 15$ and $t = 30$ years was calculated based on analysis of angle borings extracted from the Kansas City PRB. The inverted noisy data sets were characterized by a standard deviation of 0.05 (fractional error) in the resistance and a standard deviation of 1 mV/V (absolute error) in the chargeability.

May 2005 and March 2004 data sets. A positive-percentage change indicates an increase in conductivity in May 2005 relative to March 2004. As shown in Figure 6, the differences in phase between these two times (Figure 6f) are not significantly greater than the errors within each data set (Figure 6d and e). Consequently, a ratio image for the imaginary conductivity is not shown. The small difference between the measured resistances for the two data sets (Figure 6c) is manifested as a slight increase in real conductivity (less than 10%) focused within the uppermost section of the barrier on its up-gradient side.

DISCUSSION

Our synthetic studies, guided by laboratory measurements on cores of the Kansas City PRB, illustrate that it is feasible to use electrical imaging as a long-term, noninvasive monitoring tool for detecting precipitation that typically causes barrier performance reduction. The 15- and 30-year simulations conducted here reveal that it is impossible to resolve accurately the geometry of the reacted front that develops on the up-gradient face of the barrier because it is too thin. However, there is a detectable σ' anomaly in the image structure inside the barrier that essentially represents a blurred (smoothed) depiction of the model for the reacted front. The inver-

sion correctly maps the changes in the data caused by the reacted front to the internal structure of the barrier and close to the up-gradient side. Thus, we propose that this response is diagnostic of the development of a reacted front and is a distinctive signature relative to changes in the image that we anticipate would occur from changes in the antecedent conditions — water content, salinity, and temperature — outside of the barrier.

It is important to note that the a priori information provided by the regularization disconnect (whereby the regularization between the part of the FEM representing the internal structure of the barrier and the remainder of the FEM is decoupled) is critical in resolving this increase in conductivity inside the PRB structure. Without this constraint, the inversion fails to resolve an anomaly associated with the internal structure of the PRB on its up-gradient edge. For the sake of brevity, we have not shown images obtained without this disconnect threshold. We note that this disconnect method may be similarly appropriate for imaging other types of engineered structures such as containment walls or buried tanks in the unique case in which the outline of the engineered structure is known precisely, and it is the internal variability in the structure that is of interest.

Our field studies show that the geometry and internal structure of a real PRB emplacement are well resolved when using a disconnect in the regularization based on the engineered design. We assume that

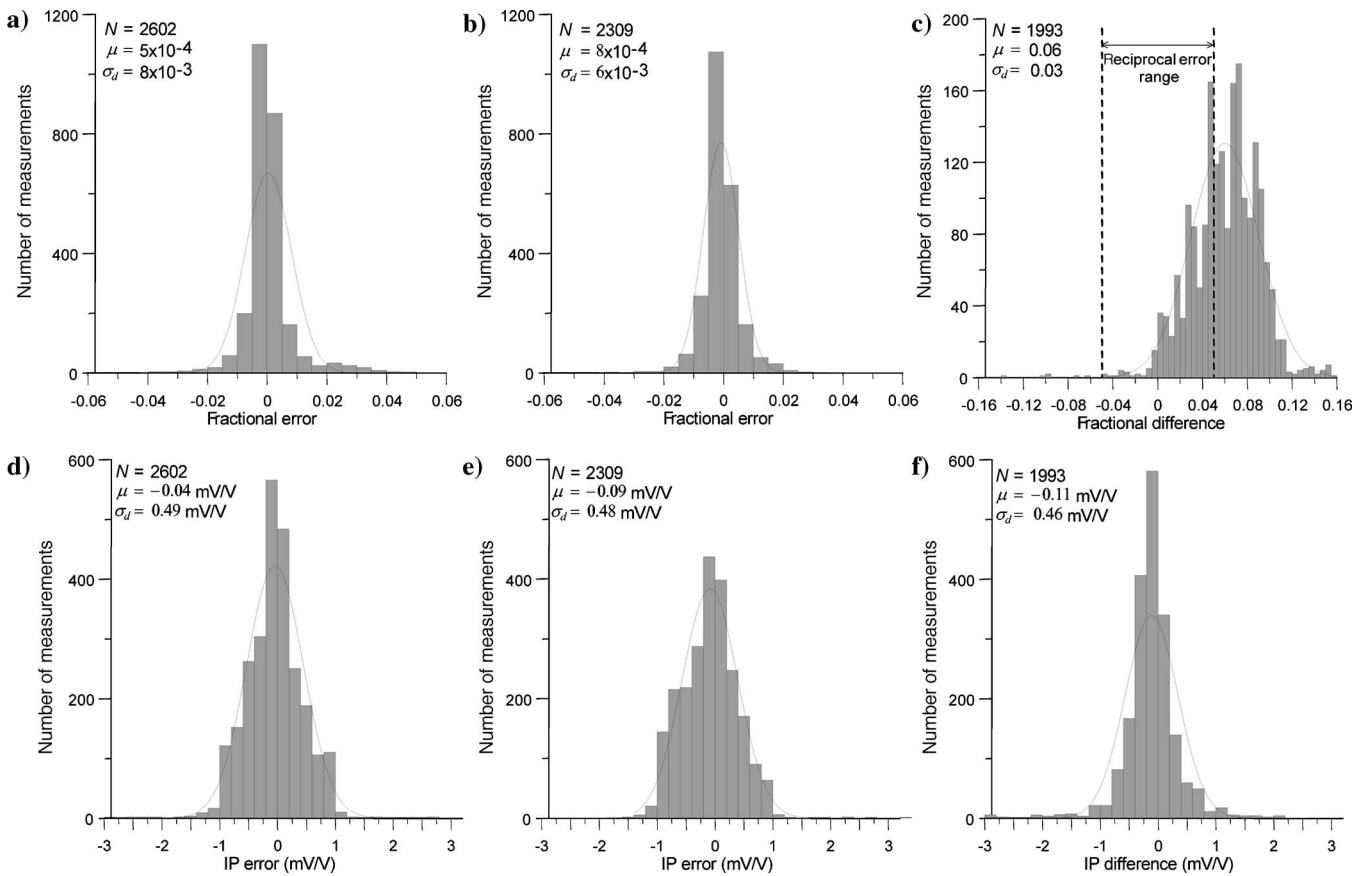


Figure 6. Histogram analysis of the reciprocal errors in the March 2004 and May 2005 data sets as well as the differences between the two data sets. The resistances are shown as fractional errors, whereas the IP measurements are shown as absolute errors. (a) March 2004 resistance reciprocals, (b) May 2005 resistance reciprocals, (c) difference in the resistances between the May 2005 and March 2004 data sets, (d) March 2004 IP reciprocals, (e) May 2005 IP reciprocals, and (f) difference in the IP measurements between the May 2005 and March 2004 data sets. The number of measurements N , mean μ , standard deviation σ_d , and normal distribution are shown for each data set. Note the difference in the scales in plot (c) relative to plots (a) and (b).

the design accurately reflects the in situ installation. The inverted field data generally produce a uniform PRB structure with only minor artifacts. Without the disconnect, we are unable to resolve such a uniform PRB structure as demonstrated in our earlier work on the same barrier (Slater and Binley, 2003). Although in this earlier study the general shape of the PRB was resolved by inverting the conductivity magnitudes, significant artifacts existed — most notably an apparent gap in the PRB between its upper and lower segments (see Figure 5 of Slater and Binley, 2003). Inversion of the induced-polarization data without the disconnect constraint did not produce convincing images of the PRB structure (see Figure 7 of Slater and Binley, 2003).

In contrast, the induced-polarization inversion with the disconnect resolves a uniform 20+ mrad structure with apparently minimal artifacts. Interestingly, the PRB is imaged as significantly more conductive (2–10 S/m) than what we measured for cores in the laboratory (0.1–1 S/m). This might reflect limitations of comparing a core-scale measurement to a field-scale structure or perhaps represent a physical effect associated with increased Fe^0 grain-grain contact because of the in situ overburden pressure that was not simulated in the laboratory. Because ϕ and conductivity magnitude are inversely related, the ϕ measured for the field PRB is similarly less than that obtained for the synthetic structure based on the laboratory data.

Predictably, the field data show little evidence for change in the electrical properties of the PRB over our 14-month interval when compared with the synthetic studies based on 15- and 30-yr monitoring periods. Laboratory measurements on cores from the PRB indicate that the 14-month sampling interval in the field is too small to expect any significant growth in the reacted front that would be detectable with electrical imaging. However, it is interesting to note that ratio images do show a small increase in conductivity inside the PRB with time (over 14 months) that occurs at a location consistent with where the synthetic images exhibit changes when modeling a

reacted front on the up-gradient edge of the PRB (compare Figures 5 and 7). It is also noteworthy that the laboratory and field results both suggest that changes in the real conductivity resulting from development of a reacted front are greater than changes in imaginary conductivity. The increase in real conductivity is attributable to an increase in electronic conduction through the granular iron mix that develops from the extensive iron-mineral precipitation exhibited in Figure 3b. Our work implies that resistivity imaging alone may be sufficient for long-term monitoring of precipitation leading to reduced PRB performance. In fact, the induced-polarization images obtained from the synthetic modeling exhibited no evidence of the reacted front and even displayed false low imaginary conductivity along the very front edge of the barrier.

Our analysis has been based principally on our interpretation of images or changes in an image over time. We recognize that the inversion process will limit such interpretation because artifacts may be introduced during this step, and errors in the inverse model will exist because of limited sensitivity and resolution of the method. We have attempted to address this by constraining the electrical images to satisfy the likely contrasts in properties at the barrier boundary; however, as Figure 5 shows, the likely changes within the barrier may be difficult to recover. An alternative approach is to constrain the process further by considering any likelihood of different model structures that represent realistic changes within the barrier. This may be addressed by searching a finite set of forward models and would remove the need for any model inversion. We believe that such approaches ultimately may offer more useful analysis for investigating engineered systems such as PRBs.

Still it is assumed often that induced-polarization measurements only can be made using nonpolarizing electrodes composed of a metal in contact with an electrolyte of the same metal. Our error analyses and repeat measurements over a 15-month period show that it is possible to obtain surprisingly high-quality IP data from field-

scale cross-borehole surveys using simple metal (in this case, lead) electrodes. The high accuracy in this IP measurement is obtained because the resistivity instrument employed has high input impedance and incorporates signal processing to estimate and remove electrode polarization at the potential electrodes prior to current injection. Simple metal electrodes are deployed readily in cross-borehole studies and are more amenable to long-term monitoring applications. We consider the present constraints on adopting electrical imaging for long-term monitoring to include such issues as long-term durability of the deployed electrode arrays and long-term electrode stability under changing geochemical conditions. Other factors include adequately accounting for changes in aqueous geochemistry that may occur over decadal timescales, thus affecting the electrical measurements.

CONCLUSION

In summary, we conclude that electrical imaging is a viable technology for monitoring the long-term decadal scale changes in the electrical properties of a PRB that result from corrosion and precipitation. Because precipitation is a major

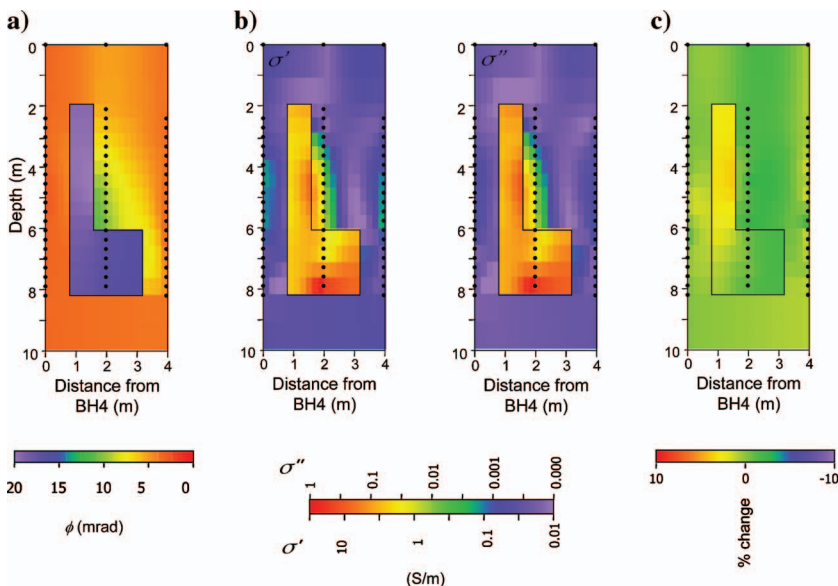


Figure 7. Results of electrical-imaging measurements at the Kansas City PRB. The inversion of the March 2004 data set (2223 measurements) is shown as (a) phase and (b) real (σ') and imaginary (σ'') conductivity. Part (c) shows an inversion for percentage changes in σ' in the May 2005 data set relative to the March 2004 data set (1993 measurements). Field data sets were characterized by a standard deviation of 0.05 (fractional error) in the resistance and a standard deviation of 1 mV/V (absolute error) in the chargeability.

cause of performance reduction, electrical imaging appears to be a viable technology for detecting and/or predicting when the PRB will fail to meet design standards for contaminant treatment. With more than eighty PRBs in operation worldwide, applying this geophysical technology could significantly impact remediation operations.

REFERENCES

- Binley, A., and A. Kemna, 2005, Electrical methods, *in* S. Hubbard and Y. Rubin, eds. *Hydrogeophysics*: Springer Publishing Company, Inc., 129–156.
- Carey, M. A., B. A. Fretwell, N. G. Mosley, and J. W. N. Smith, 2002, Guidance on the design, construction, operation and monitoring of permeable reactive barriers, NC/01/51, Environment Agency, U. K.
- Dahlin, T., V. Leroux, and J. Nissen, 2002, Measuring techniques in induced polarisation imaging: *Journal of Applied Geophysics*, **50**, 279–298.
- Daily, W., and E. Owen, 1991, Cross-borehole resistivity tomography: *Geophysics*, **56**, 1228–1235.
- Daily, W., and A. Ramirez, 2000, Electrical imaging of engineered hydraulic barriers: *Geophysics*, **65**, 83–94.
- Daily, W., A. Ramirez, R. Newmark, and V. George, 2000, Imaging UXO using electrical impedance tomography: *Journal of Environmental and Engineering Geophysics*, **5**, 11–24.
- de Groot Hedlin, C., and S. Constable, 1990, Occam's inversion to generate smooth, two dimensional models from magnetotelluric data: *Geophysics*, **55**, 1613–1624.
- Furukawa, Y., J. W. Kim, J. Watkins, and R. T. Wilkin, 2002, Formation of ferrihydrite and associated iron corrosion products in permeable reactive barriers of zero-valent iron: *Environmental Science and Technology*, **36**, 5469–5475.
- Gavaskar, A. R., N. Gupta, B. M. Sass, R. J. Janosy, and D. O'Sullivan, 1998, *Permeable reactive barriers for groundwater remediation*: Batelle Press.
- Gilham, R. W., and S. F. O'Hannesin, 1994, Enhanced degradation of halogenated aliphatics by zero valent iron: *Ground Water*, **32**, 958–967.
- Gu, B., L. Liang, M. J. Dickey, X. Yin, and S. Dai, 1998, Reductive precipitation of uranium(VI) by zero-valent iron: *Environmental Science and Technology*, **32**, 3366–3373.
- Gu, B., T. J. Phelps, L. Liang, M. J. Dickey, Y. Roh, B. L. Kinsall, A. V. Palumbo, and G. K. Jacobs, 1999, Biogeochemical dynamics in zero-valent iron columns: Implications for permeable reactive barriers: *Environmental Science and Technology*, **33**, 2170–2177.
- Joesten, P. K., J. W. Lane, J. G. Savoie, and R. J. Versteeg, 2001, Application of borehole-radar methods to image two permeable reactive-iron walls at the Massachusetts Military Reservation, Cape Cod, Massachusetts: *Proceedings of the Symposium on the Application of Geophysics to Engineering and Environmental Problems*, Environmental and Engineering Geophysical Society.
- Kemna, A., 2000, *Tomographic inversion of complex-resistivity — Theory and application*: Der Andere Verlag.
- Kemna, A., and A. Binley, 1996, Complex electrical resistivity tomography for contaminant plume delineation: *Proceedings of the 2nd Meeting of Environmental and Engineering Geophysics*, European Environmental and Engineering Geophysical Society, 196–199.
- Kemna, A., A. Binley, and L. Slater, 2004, Cross-borehole IP imaging for engineering and environmental applications: *Geophysics*, **69**, 97–107.
- Klausen, J., P. J. Vikesland, T. Kohn, D. R. Burris, W. P. Ball, and A. L. Roberts, 2003, Longevity of granular iron in groundwater treatment processes: Solution composition effects on reduction of organochlorides and nitroaromatic compounds: *Environmental Science and Technology*, **37**, 1208–1128.
- Kohn, T., K. J. T. Livi, A. L. Roberts, and P. J. Vikesland, 2005, Longevity of granular iron in groundwater treatment processes: Corrosion product development: *Environmental Science and Technology*, **39**, 2867–2879.
- LaBrecque, D. J., M. Miletto, W. Daily, A. Ramirez, and E. Owen, 1996, The effects of noise on Occam's inversion of resistivity tomography data: *Geophysics*, **61**, 538–548.
- Legrand, L., M. Abdelmoula, A. Gehin, A. Chausse, and J. M. R. Genin, 2001, Electrochemical formation of a new Fe(II)-Fe(III) hydroxy-carbonate green rust: Characterisation and morphology: *Electrochimica Acta*, **46**, 1815–1822.
- Liang, L. Y., N. Korte, B. H. Gu, R. Puls, and C. Reeter, 2000, Geochemical and microbial reactions affecting the long-term performance of in situ 'iron barriers': *Advances in Environmental Research*, **4**, 273–286.
- Liang, L. Y., A. B. Sullivan, O. R. West, G. R. Moline, and W. Kamolpornwijiit, 2003, Predicting the precipitation of mineral phases in permeable reactive barriers: *Environmental Engineering Science*, **20**, 635–653.
- Mackenzie, P. D., D. P. Horney, and T. M. Sivavec, 1999, Mineral precipitation and porosity losses in granular iron columns: *Journal of Hazardous Materials*, **68**, 1–17.
- Oldenburg, D. W., and Y. Li., 1994, Inversion of induced-polarization data: *Geophysics*, **59**, 1327–1341.
- Park, S. K., and G. P. Van, 1991, Inversion of pole-pole data for 3-D resistivity structure beneath arrays of electrodes: *Geophysics*, **56**, 951–960.
- Phillips, D. H., B. Gu, D. B. Watson, Y. Roh, L. Liang, and S. Y. Lee, 2000, Performance evaluation of a zerovalent iron reactive barrier: Mineralogical characteristics: *Environmental Science and Technology*, **34**, 4169–4176.
- Ramirez, A., W. Daily, A. Binley, D. LaBrecque, and D. Roelant, 1996, Detection of leaks in underground storage tanks using electrical resistance methods: *Journal of Environmental and Engineering Geophysics*, **1**, 189–203.
- Shima, H., 1992, 2-D and 3-D resistivity image reconstruction using cross-hole data: *Geophysics*, **57**, 1270–1281.
- Slater, L., and A. Binley, 2003, Evaluation of permeable reactive barrier (PRB) integrity using electrical imaging methods: *Geophysics*, **68**, 911–921.
- Slater, L., A. Binley, W. Daily, and R. Johnson, 2000, Cross-hole ERT imaging of a controlled tracer injection: *Journal of Applied Geophysics*, **44**, 85–102.
- Slater, L., J. Choi, and Y. Wu, 2005, Electrical properties of iron-sand columns: Implications for induced-polarization investigation and performance monitoring of iron-wall barriers: *Geophysics*, **70**, G87–G94.
- Su, C., and R. Puls, 2004, Significance of Iron (II, III) hydroxycarbonate green rust in arsenic remediation using zerovalent iron in laboratory column tests: *Environmental Science and Technology*, **38**, 5224–5231.
- U. S. Department of Energy, 2003, *Annual groundwater corrective action report*: Honeywell Federal Manufacturing and Technologies.
- Vogan, J. L., R. M. Focht, D. K. Clark, and S. L. Graham, 1999, Performance evaluation of a permeable reactive barrier for remediation of dissolved chlorinated solvents in groundwater: *Journal of Hazardous Materials*, **68**, 97–108.
- Wu, Y., L. Slater, and N. Korte, 2005, Effect of precipitation on low frequency electrical properties of zero valent iron: *Environmental Science and Technology*, **39**, 9197–9204.